PHYSICAL REVIEW B VOLUME 25, NUMBER 2 15 JANUARY 1982

Charge-density-wave motion in $NbSe_3$. II. Dynamical properties

J. Richard, P. Monceau, and M. Renard
Centre de Recherches sur les Très Basses Températures, Centre National de la Recherche Scientifique, B.P. 166 X, 38042 Grenoble-Cedex, France
(Received 4 May 1981)

We have studied the quasiperiodic noise generated in $NbSe_3$ above the critical electric field where the charge-density waves (CDW's) are depinned. The Fourier spectrum of the noise can be totally described with three fundamental frequencies and their harmonics. At high electric fields the fundamental frequencies are still observable at 100 MHz. We have performed interferences between these frequencies in the noise and an external rf field as measured in the low-frequency dV/dI characteristic. With the model where the phase of the CDW is described as an overdamped oscillator we explain why we observe an increase in the differential resistance of the periodic frequencies. We explain also that, in spite of the great number of domains in the sample, a coherent signal is observed because of the self-synchronization of all the domains at a given frequency. We show that the periodic frequency has a linear variation with the current carried by the CDW. The inverse of this slope gives the number of electrons in the band affected by the CDW gap. We find that this number is the same for each CDW in $NbSe_3$ and in excellent agreement with the number of electrons which can be obtained by simple band calculations.

I. INTRODUCTION

One of the aims in the study of dimensionality-restricted systems, in particular one-dimensional systems, concerns the possibility of observing superconductivity by another mechanism than the one described by the theory of Bardeen, Cooper, and Schrieffer[1] (BCS). In fact, one year before the BCS theory, Frölich[2] had proposed a model where a charge-density wave (CDW) could move without damping in the lattice if its phase were invariant by translation. Lee, Rice, and Anderson[3] showed that in real systems the phase of the CDW was pinned by commensurability with the underlying lattice, or by Coulomb interactions between adjacent chains or by impurity pinning. Oscillations of the CDW around the pinning centers can explain the large values of the dielectric constant in K_2 [$Pt(CN)_4$] $Br_{0.3}\cdot 3H_2O$ [KCP (Ref. 4)] and in tetrathiafulvalene-tetracyanoquinodimethane (TTF-TCNQ).[5] Conductivity nonlinear with the applied electric field has been observed at very low temperature in the insulating Peierls phase of one-dimensional (1D) conductors and explained by nonlinear excitations or solitons in the CDW lattice.[5] A drop in longitudinal conductivity of TTF-TCNQ has been observed in the pressure range where the CDW and the lattice are commensurable and therefore when the CDW is more strongly pinned. This result suggests a contribution of mobile CDW fluctuations to the conductivity above the Peierls transition when the CDW and the lattice are incommensurable.[6] However, $NbSe_3$ is unique because it shows an extraconductivity induced by the electric field[7] in the full range of temperature where two incommensurable CDW transitions appear at $T_1 = 145$ K and $T_2 = 59$ K, which was associated with the motion of the CDW's.[8] Unfortunately, superconductivity was not observed, and the maximum of conductivity measured is no larger than that which can be deduced if the CDW's were not present. However, $NbSe_3$ is not a strictly 1D material, and normal electrons remain after the two successive gaps induced by the CDW's.

As found by Fleming and Grimes,[9] the nonlinear properties start above a critical electric field when the electric force overcomes the pinning force. In paper I (Ref. 7) we have reported measurements of the differential resistance variation dV/dI as a function of the current in the sample, and we have shown that under some conditions a sharp dip in dV/dI is observed near the critical field. We have developed a model where, in a domain, the CDW

follows two equations: Its phase is described as an overdamped oscillator, and the total current is the sum of the normal electron current and the current carried by the CDW in motion. We have solved these equations by assuming either the electric field or the current regulated. Discrepancies between the experimental results and the model with a unique domain have led us to consider that the sample is formed with multiple domains in which the phase of the CDW is constant, each domain separated from another by normal walls. This description is supported by the observation of domains by Fung and Steeds[10] and by the filamentary superconductivity[11] measured at low temperature. We have assumed that the distribution of critical electric fields of this assembly of domains was Gaussian.

Above the critical field noise is generated in the crystal. Fleming and Grimes[9] have shown that this noise is the superposition of a broad-band noise and a periodic noise. We have interpreted these frequencies as the modulation of the current carried by the CDW in the pinning potential.[12] We previously reported the observation of steps in the nonlinear characteristic when we superpose a rf field with variable frequency and a given dc current higher than the critical one. These steps or peaks in dV/dI are the consequence of the synchronization of the noise by the external rf field.

Hereafter we describe in detail experiments on the quasiperiodic noise. We have performed synchronization experiments for the two CDW's and have studied the influence of the rf amplitude on the observation of harmonics and subharmonics. We have also analyzed directly the noise with a spectrum analyzer, and we show that except near the critical field the frequencies measured in the dV/dI characteristics with the external synchronization and those measured by direct analysis of the noise are identical. All the quasiperiodic noise can be described with three fundamental frequencies with harmonics and subharmonics. With the same model as that in paper I, we explain why we observe an *increase* in the differential resistance at the periodic frequencies. We also explain that the coherent signal measured between the voltage leads, in spite of the great numbers of domains in the sample, results from the locking of all the domains at a given frequency. Finally, we verify the linear variation of the frequencies with the current carried by the CDW. The slope measures the number of electrons in the band affected by the gap. We find that the same number of electrons is involved in each CDW, and this number is in excellent agreement with that which is deduced at room temperature by band calculations.

II. EXPERIMENTAL TECHNIQUES

The characteristics of the samples that we have measured are indicated in Table I of paper I. The technique of synchronization of the quasiperiodic noise by an external rf field is shown in the block diagram of Fig. 1. The rf generator delivers a variable frequency which is swept linearly with time. The amplitude of the rf current is measured through the resistance R with an oscilloscope. The frequency is measured with the frequencemeter and is recorded through a digital analogic converter on an x-y recorder. The differential resistance is obtained with four contacts with an ac bridge working at 33 Hz where the ac current can be varied between 0.01 and 10 μA (typically 1 μA). Any parasitic reflections in the current leads between 20 kHz and 20 MHz were eliminated with adequate inductances and capacitances.

For the direct analysis of the noise across the sample, the voltage noise was amplified with a differential amplifier with a bandpass of 2 MHz and analyzed with a 7L5 Tektronix spectrum analyzer. The eigenfrequencies are directly visualized on the oscilloscope and can be drawn on an x-y recorder by sweeping the frequency. When the contacts were made with silver paint as for sample 1 or for sample 5, the Fourier-spectrum analysis led to frequencies that were not very well defined but asymmetrical and broad. When the contacts were made by pressure between the sample and gold evaporated leads on a quartz substrate, as for sample 6, very sharp peaks were observed in the Fourier analysis, perhaps because of the better definition of the equipotentials at the voltage contacts. Therefore for sample 6, we have extended the noise analysis with the 7L13 Tektronix spectrum analyzer where the central frequency can be varied between 100 kHz and 1.8 GHz. The noise voltage is amplified with a broad-band amplifier which is not differential, but we have verified separately for each voltage lead that the same spectrum was obtained. We have observed fundamental frequencies up to 100 MHz and harmonics up to 400 MHz.

We have studied the two CDW's in $NbSe_3$. The measurements for the upper CDW were performed in liquid argon to eliminate any heating problems

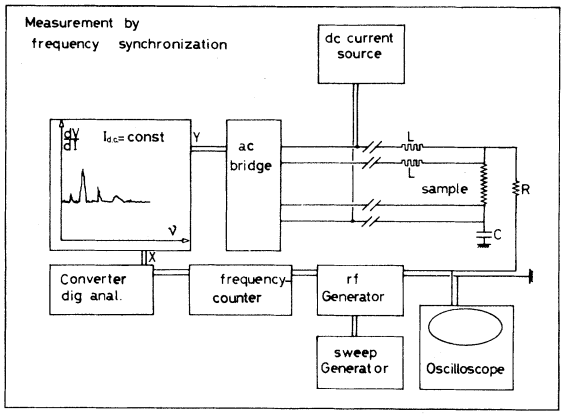

FIG. 1. Block diagram of the synchronization experiment between an external rf frequency and the voltage noise induced in the nonlinear state of $NbSe_3$.

and for the lower CDW in regulated helium-gas flow.

III. EXPERIMENTAL RESULTS

A. Synchronization of the periodic noise by an external rf field

In Fig. 2 we emphasize the effect of the superposition of a rf current and a dc current for the upper CDW transition. We applied to the sample a rf current with a constant amplitude and a fixed frequency, and we swept the dc current. The differential resistance (at 33 Hz) shows the same features as reported in paper I in Fig. 2: dV/dI is constant up to a critical electric field E_c (or a critical current because we are in the current-regulated

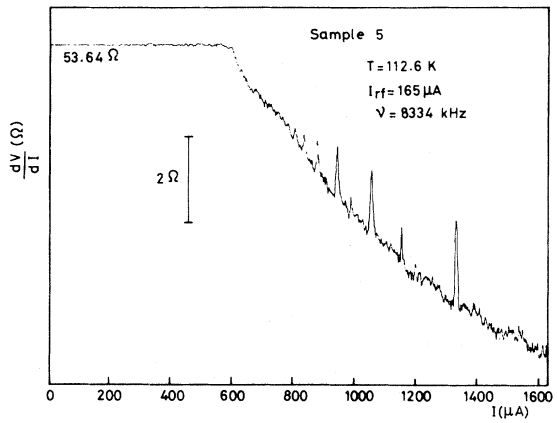

FIG. 2. Differential resistance dV/dI (at 33 Hz) as a function of the current swept in the sample with a 8.334-MHz rf field applied. Peaks indicate synchronization of the noise frequencies with the external frequency.

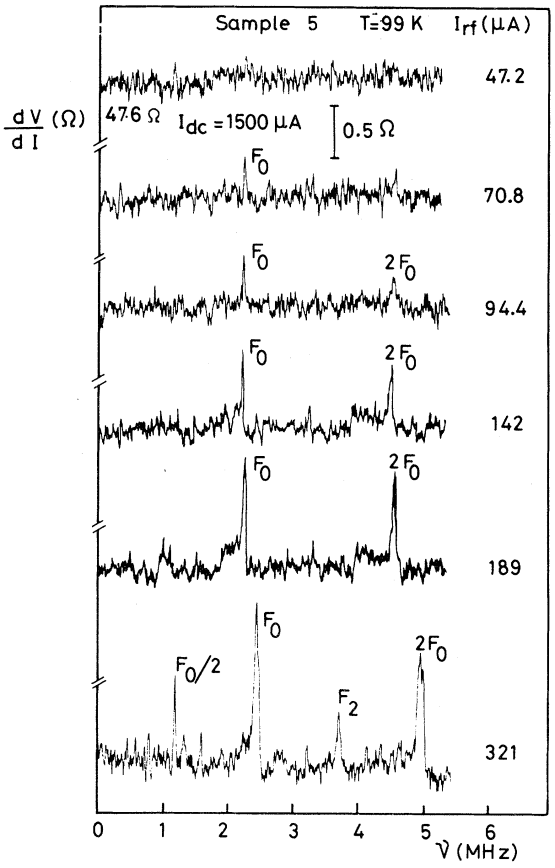

FIG. 3. Differential resistance dV/dI as a function of the external frequency for an electric field $E/E_c(I_{rf}=0) = 1.57$ at different amplitudes of the rf current. The fundamental frequency peak in dV/dI appears only when $I_{rf} > 70.8$ μA. For higher rf amplitudes, harmonics and subharmonics of F_0 are observed.

regime) above which the pinning is overcome. Above E_c, dV/dI decreases. However, the effect of the rf field is characterized by the presence of several peaks. As explained in paper I, in the depinned regime the current carried by the CDW has an ac component which is a function of the electric field in the sample. When the frequency of this modulated current is equal to the externally applied rf frequency there is interference, as seen by an increase in dV/dI. In practice we do not perform the experiments in this way, but we keep constant the dc current higher than both the critical current and the amplitude of the rf current, and we sweep the frequency of this rf current.

1. *Effect of the amplitude of the rf field*

The observation of peaks in the variation of dV/dI with the external frequency requires the rf

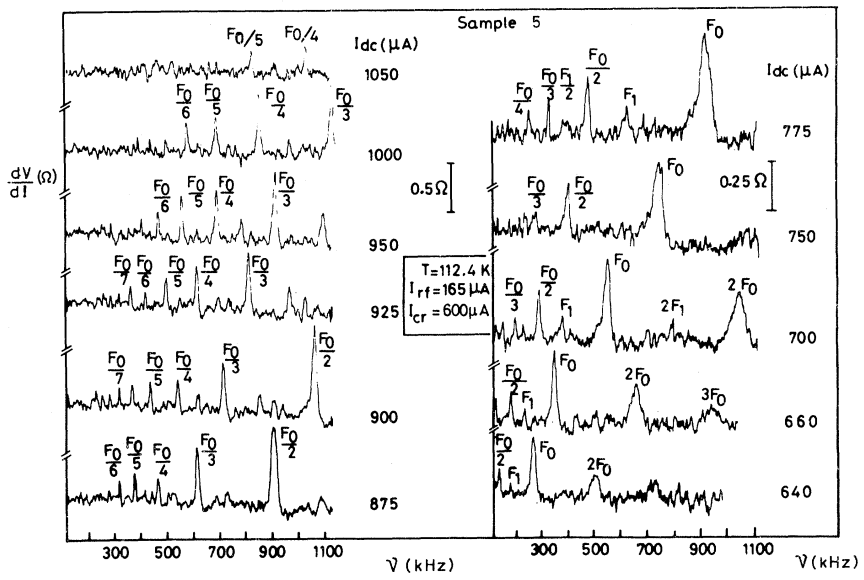

FIG. 4. Differential resistance dV/dI as a function of the external frequency in the 0.1—1.1 MHz range for sample 5 at 112.4 K with a constant rf amplitude and for different dc currents higher than the critical one. All the peaks are labeled as harmonics or subharmonics of the fundamental F_0 and two fundamental satellites F_1 and F_2.

current to be at a certain minimum. In Fig. 3 we show the variation of dV/dI for the upper CDW transition of sample 5 at different rf currents for $E/E_c(I_{rf}=0)=1.57$. We observe that below the rms amplitude of the rf current of 71 μA, there is no peak. For higher rf values, one peak appears. For the following we will call as the fundamental frequency the *first* frequency F_0 which appears when we increase the amplitude of the rf field. For all the samples studied and all the temperatures, the ratio between the rf electric field and the dc electric field in the sample for observing the fundamental frequency in dV/dI is around 6%. When the rf current is increased further, the am-

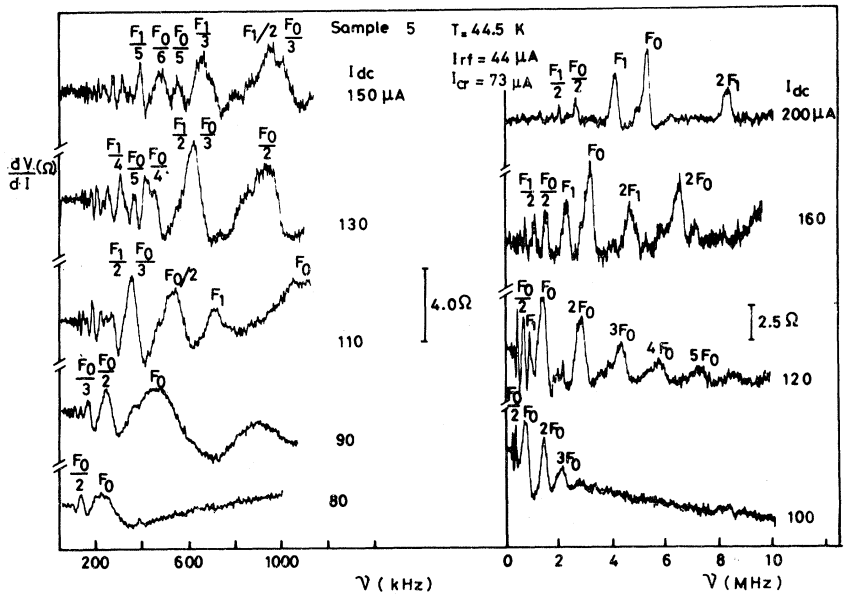

FIG. 5. Same as Fig. 4 but for $T=44.5$ K. The left-hand part: the 0.1—1.1 MHz frequency range. The right-hand part: between 0.1 and 10 MHz.

plitude of the fundamental frequency increases, harmonics and subharmonics appear, and also two other frequencies F_1 and F_2 are observed. We have verified that the amplitude of F_0 (or F_1 and F_2) saturates at high rf currents. When the rf field is not too strong compared to the dc electric field, the frequencies of the fundamental and its harmonic are independent of the rf current which is not the case with too high a rf current (321 μA in Fig. 3) or near the critical field. However, as it was shown in paper I, Sec. III E the depinning conditions are changed when we superpose a high-amplitude rf field at a relatively low frequency ($\sim$1 MHz). The dc critical field is reduced, and therefore for the same applied field, following Eq. (11) in paper I, synchronization takes place at higher frequencies.

2. *Variation of $\frac{dV}{dI}$ with the external frequency*

In Fig. 4 we show the variation of dV/dI concerning the upper CDW transition of sample 5 as a function of the external applied frequency in the 0.1$-$1.1 MHz range for different dc currents higher than the critical current. At 112.4 K, $E_c = 600$ μA as seen in Fig. 2. We note that all the frequencies increase with the dc current (or the dc electric field). All the peaks in dV/dI can be labeled as harmonics or subharmonics of F_0 and also of another frequency F_1. With the rf amplitude applied, $E_{rf}/E_c = 0.275$, many subharmonics of F_0 (at least seven) are observed.

Figure 5 shows the same dV/dI variation as that in Fig. 4 but for the lower CDW transition, where the same features are observed. In the left-hand part of Fig. 5 in the 0.1$-$1 MHz range all the peaks are labeled as harmonics and subharmonics of F_0 and F_1. In the right-hand part of Fig. 5 for higher electric fields we see that the subharmonic content decreases. However, the experiments were performed with a constant value of I_{rf} and we have seen in Sec. III A 1 that the important parameter for the observation of subharmonics is the ratio E_{rf}/E, so at high E the subharmonic amplitude decreases, and only the fundamental frequencies remain. However, if we increase E_{rf} we observe again many subharmonics.

In Fig. 6 we show the variation of dV/dI at high electric fields compared with the critical field for the two CDW's in the 0.1$-$20 MHz frequency range. The amplitude of harmonics when observed is just slightly decreasing when their range is higher. We have reported previously[12] that the peaks in dV/dI disappeared for 3 or 4 E_c, only because the rf amplitude was kept too small. For sample 6 we have observed frequencies and harmonics up to $10E_c$.

3. *Temperature variation of $\frac{dV}{dI}$*

The variation of dV/dI as a function of the rf frequency is totally similar for the two CDW's. We have observed that the peaks in dV/dI are very broad in the temperature range between T_{c_1} or

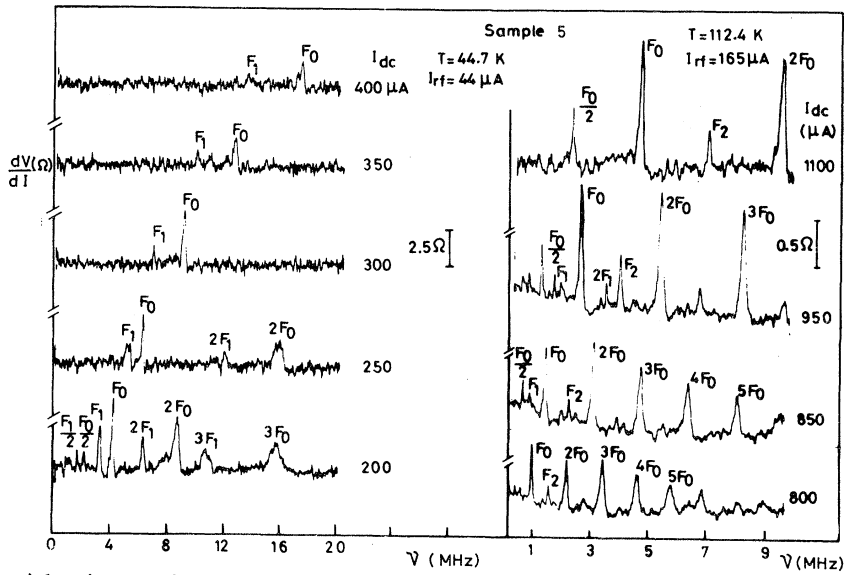

FIG. 6. Differential resistance dV/dI as a function of the external frequency in the range 0.1$-$20 MHz for sample 5 at $T = 44.7$ and 112.4 K.

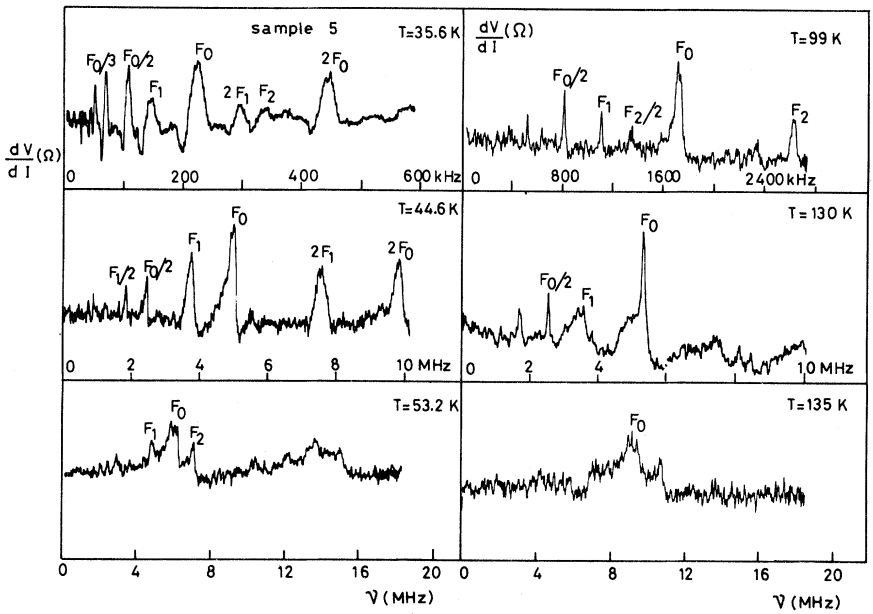

FIG. 7. Differential resistance dV/dI as a function of the external frequency with approximately the same reduced temperatures compared to the two CDW formations $T_1=145$ K and $T_2=59$ K. Near $T_{c_{1,2}}$ peaks are very broad and become sharp at low reduced temperature.

T_{c_2} and the temperature where the resistivity is maximum. If we define a Q of the "resonances" as measured at the middle of the peaks, near T_{c_1} or T_{c_2}, Q is typically around 3, but below the resistance maximum temperature Q is around 50. To illustrate this point in Fig. 7 we show dV/dI at different temperatures for each CDW for approximately the same $T/T_{c_{1,2}}$.

Thus by the application of a rf field, resonances are observed in dV/dI which are harmonics or subharmonics of three fundamental frequencies (in the following the peaks are represented by the

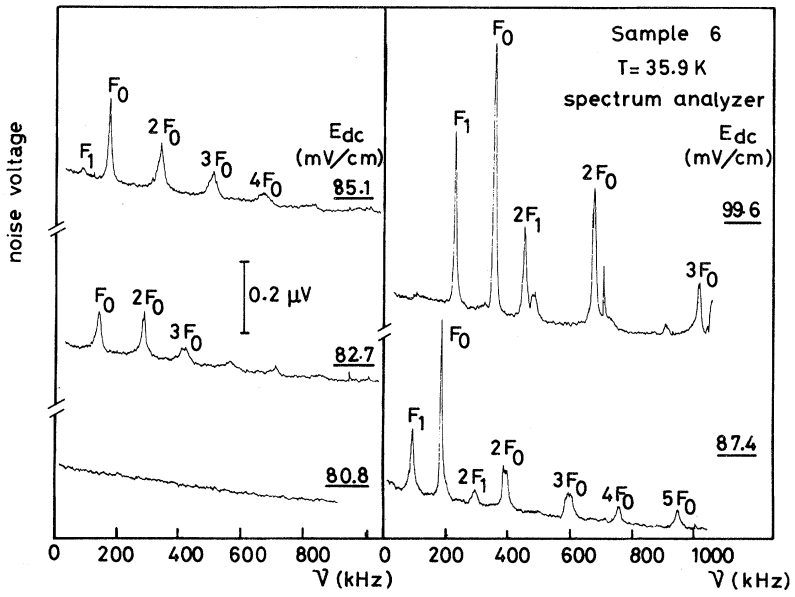

FIG. 8. Fourier spectrum obtained by direct noise analysis with a spectrum analyzer for sample 6 at $T=35.9$ K. The critical field is $E_c=80.4$ mV/cm. Fundamental frequency F_0 appears at a *finite* value at E_c, then F_1 and F_2. This behavior is directly related to the shape of the dV/dI variation which shows a discontinuity at E_c (see paper I).

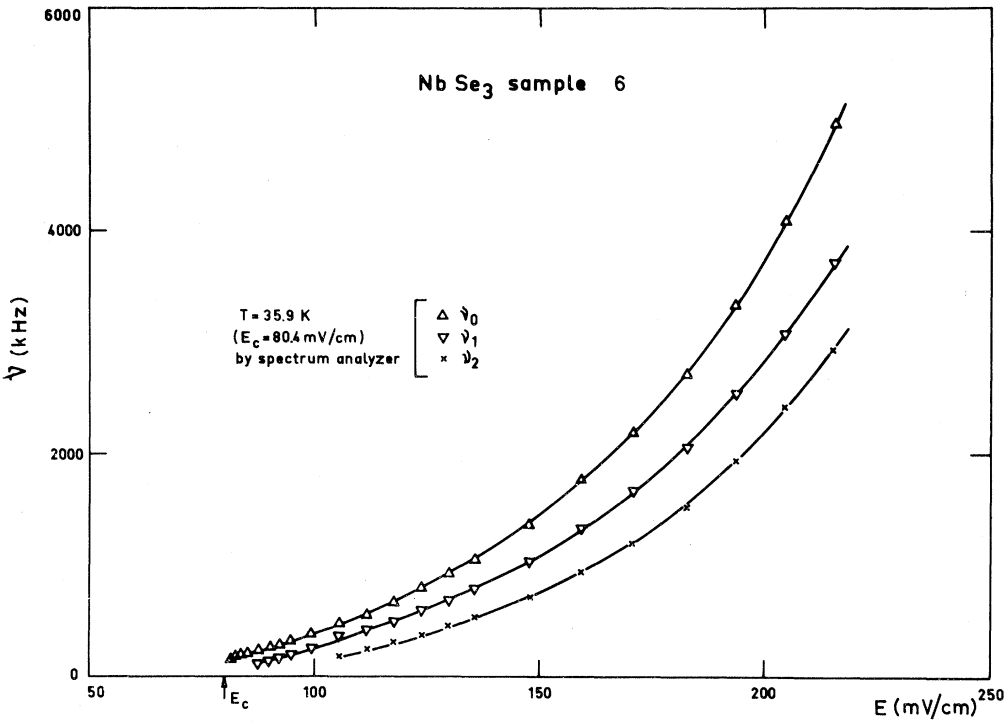

FIG. 9. Variation with the electric field of the three fundamental frequencies ν_0,ν_1,ν_2 which appear in the noise at $T=35.9$ K for sample 6.

letters F_0,F_1,F_2 and their frequencies by ν_0,ν_1,ν_2).

B. Direct analysis of the periodic noise

The Fourier components of the voltage noise can be obtained directly by analyzing the noise with a spectrum analyzer as made for the first time by Fleming and Grimes[9] and later by several other groups.[12–15]

1. Finite frequency at the critical field

When the differential resistance dV/dI shows a continuous drop at the critical field as for sample 1 (Fig. 1 in Ref. 12), sample 4 (Fig. 1 in paper I), or for the samples measured by Fleming,[13] the eigenfrequency starts at zero at E_c and increases with the electric field. However, this is not the case for samples where dV/dI shows a sharp discontinuity at E_c, as does sample 6 (Fig. 6 in paper I). In Fig. 8 we show the Fourier spectrum of the noise of sample 6 at 35.9 K drawn on an x-y recorder. E_c at this temperature is 80.4 mV/cm. This field corresponds to the sharp drop in dV/dI where, as seen in paper I, broad-band noise is generated in the crystal. Just 2 mV/cm above E_c, the Fourier spectrum shows a frequency F_0 and its harmonics where the variation cannot be extrapolated to zero for E_c. As in Sec. III A we will define as the *fundamental* frequency the first frequency which appears in the Fourier analysis. When E is increased a little more, another frequency F_1 is detected with its harmonics. The third frequency F_2 will be visible for $E=105$ mV/cm. These eigenfrequencies appear at a *finite* value, F_0 at E_c and F_1 and F_2 for higher values of E. The variation of F_0,F_1,F_2 with E is shown in Fig. 9. This behavior is directly related to the shape of dV/dI. Thus for sample 6 at $T=48.6$ K where dV/dI does not show a discontinuity at E_c, F_0 extrapolates to zero at E_c.

2. Eigenfrequencies at very high electric field

The sharpness of the Fourier peaks in the noise for sample 6 between 0 and 5 MHz leads us to follow these frequencies at higher electric fields. The 7L13 Tektronix spectrum analyzer can measure frequencies up to 1.8 GHz, but its frequency definition is much less precise than the 7L5 analyzer, especially at low frequency. We have increased the

TABLE I. Noise eigenfrequencies of sample 6 at $T=48.6$ K, $E_c=46$ mV/cm. All frequencies are measured in MHz; E is measured in mV/cm.

E	ν_0	ν_1	ν_2	$2\nu_0$	$2\nu_1$	$2\nu_2$	$3\nu_0$	$3\nu_1$	$4\nu_0$	$4\nu_1$	$5\nu_0$	$5\nu_1$	$6\nu_0$	$7\nu_0$	$8\nu_0$
124.5	11.6	10.51	10	23.5	22.7	20.2		33.5	47.5	44.0	59.5	55.2	72	83.2	95.2
430.0	90.1	88.2	86.2	180.5	176.5	171.8	270.9	265.0	361.8	353					
	ν_3	ν_4	ν_5	$2\nu_3$	$2\nu_4$	$2\nu_5$									
	81	75.2	74	164	150	148									
	ν_6	ν_7													
	47.8	45.5													

electric field up to $10E_c$ above which the sample started not to be in thermal equilibrium. However, the F_0,F_1,F_2 triplet is always visible, and its amplitude does not decrease. In Fig. 10, we show the Fourier spectrum in a finite frequency range for $E/E_c \sim 10$. In addition to the F_0,F_1,F_2 triplet and its harmonics, lower frequencies (F_3,F_4,F_5), which appear also as a triplet, are visible. These lower frequencies are not subharmonics of the three fundamental frequencies. In Table I, we indicate the values of the frequencies for two different values

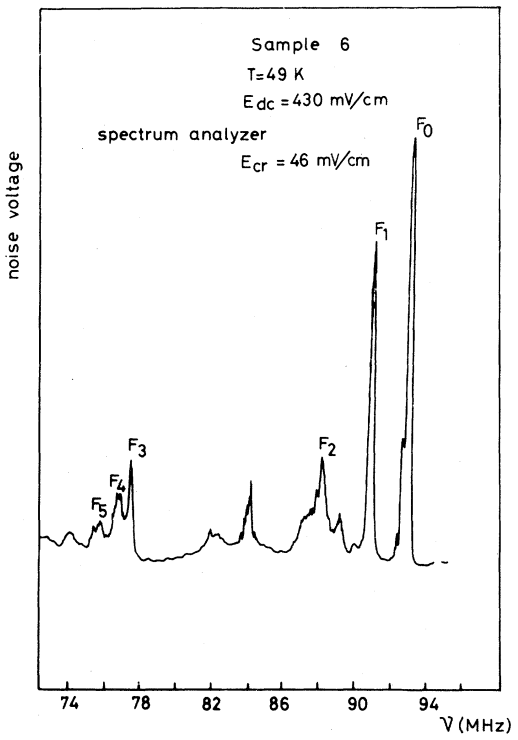

FIG. 10. Fourier spectrum of the noise induced in sample 6 for $E/E_c \sim 10$. The triplet frequencies are visible at 90 MHz. A lower frequency triplet F_3,F_4,F_5 appears at lower frequencies.

of E. We see that for $E/E_c \sim 3$ or 4, we are able to observe the 8th harmonic.

C. Variation of the eigenfrequencies with electric field

In Fig. 11 we have drawn the variation of the fundamental frequency ν_0 for the two CDW's of sample 5 as obtained in the synchronization experiment. At high electric field ν_0 is almost linear with E but the curvature near E_c is more and more pronounced when T is decreased below the CDW critical temperature. In the synchronization experiment the frequencies extrapolate to zero at E_c because the rf amplitude suppresses the sharp dip in dV/dI (as seen in Fig. 7 of paper I).

Figure 12 shows the variation of the fundamental eigenfrequency of sample 6 obtained from the synchronization experiment and the noise analysis for the lower CDW. At 48.6 K in the noise analysis ν_0 extrapolates to zero at E_c because at this temperature the dV/dI variation does not show a discontinuity, whereas ν_0 has a finite value at E_c for $T=34.9$ K. ν_0 is also independent of the rf amplitude. ν_0 obtained by the two techniques is exactly the same except for $E_c < E \lesssim 2E_c$, where the frequency obtained by synchronization is higher than that in the noise analysis. Figure 13 shows the triplet eigenfrequencies obtained in the two experiments at $T=48.6$ K. The small frequencies measured in the noise analysis near E_c correspond to frequencies in the electric range where dV/dI shows some rounding before the sharp dip (see Fig. 7 of paper I). In this range the frequencies are very small. For higher electric fields ν_0 varies rapidly and linearly with E. This slope extrapolates to zero at the same electric field E_{cr} where dV/dI drops. To illustrate the effect of the rf field near E_c we show in Fig. 14 the measured conductivity as a function of E with and

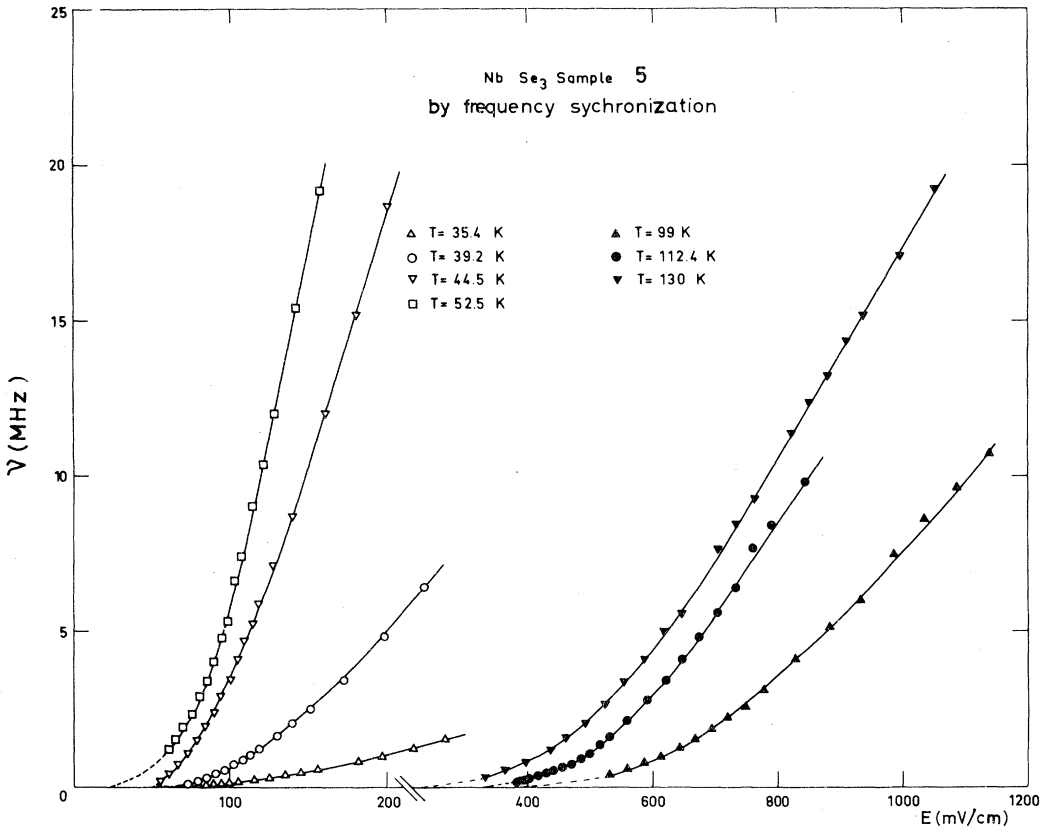

FIG. 11. Variation with the electric field of the fundamental frequency ν_0 of sample 5 measured in the synchronization experiment for different temperatures involving the two CDW's.

without a rf field. The low frequencies in the noise near E_c correspond to the electric-field range where σ increases smoothly near E_c, and the fast variation of ν with E corresponds to the electric-field range where σ increases more rapidly. The rf field suppresses this sharp variation of σ and gives a lower critical field E_c'. For a given electric field lower than E_{cr}, when we apply the rf field, the CDW is depinned and frequencies in the noise are observable.

For sample 6, Fig. 15 shows the $\nu(E)$ variation in a very large electric-field range. The linear variation seen in Fig. 12 up to 20 MHz does not hold for higher fields and an upward curvature is observed. Between $3E_c$ and $10E_c$ we can write $\nu \sim A(E-E_c)^{\alpha}$ with $\alpha \sim 1.3$, whereas Weger *et al.*[14] have reported a value of $\alpha=2$.

D. Ratio between the three fundamental frequencies

As seen in Secs. III A and III C, the whole frequency spectrum can be described with a strong amplitude fundamental frequency ν_0 and two satellite fundamental frequencies ν_1 and ν_2. For sample 6 by direct noise analysis we have shown in Fig. 9 that the frequency which appears is ν_0, then ν_1 and ν_2. We have drawn in Fig. 16 the ratios ν_0/ν_1 and ν_2/ν_1 for different temperatures as a function of E/E_c. ν_0/ν_1 and ν_2/ν_1 show a strong variation between $1<E/E_c \lesssim 2$ where the frequencies are more and more spread when E is nearer to E_c. For $E/E_c>2$, ν_0/ν_1 and ν_2/ν_0 vary smoothly towards 1. However, as seen in Fig. 10 for large values of E/E_c the three frequencies are yet distinguishable. For $T=48.6$ K (right-hand part of Fig.

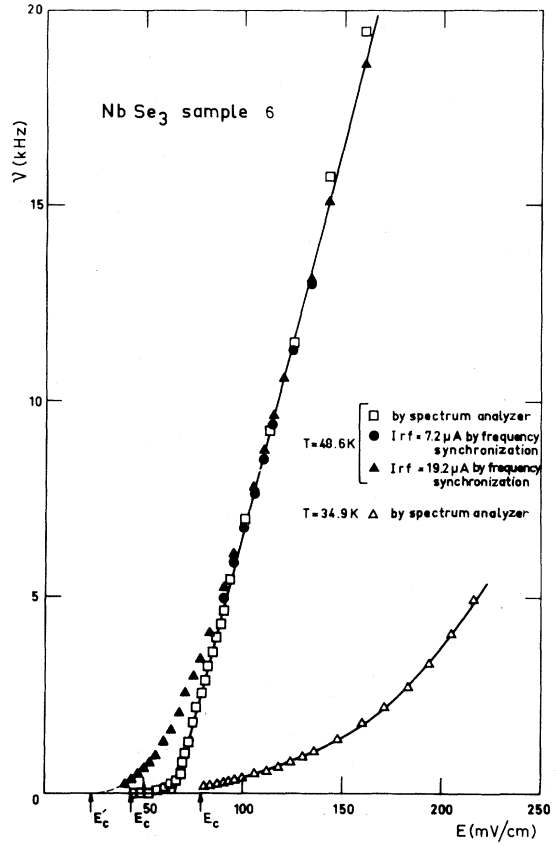

FIG. 12. Variation with the electric field of the fundamental frequency ν_0 of sample 6 obtained in the synchronization experiment and by direct analysis of the noise at $T=48.6$ K. The difference in the variation near E_c is due to the effect of the rf field on E_c and the shape of the dV/dI variation.

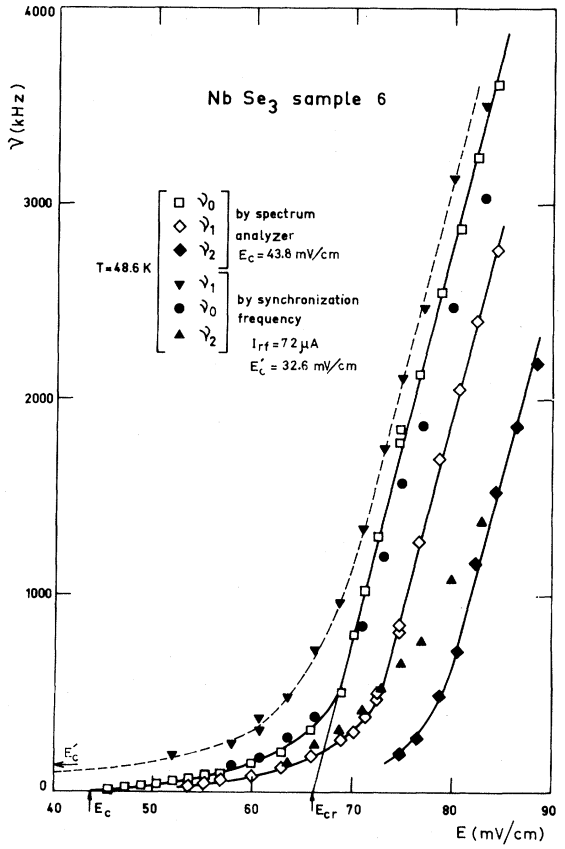

FIG. 13. Same as Fig. 12. We plot the triplet frequencies obtained in the synchronization experiment and by noise analysis near E_c. E_{c_r} is the extrapolation of the discontinuous variation of dV/dI (see Fig. 7 in paper I) and E_c' the apparent critical field with the superposition of the rf field.

16) ν_0/ν_1 shows a peak when the electric field is in the range where dV/dI has a discontinuity (Fig. 7 of paper I). At the same temperature, from synchronization experiments we have observed the same frequencies seen in Fig. 13; ν_1/ν_0 decreases smoothly and does not show a peak because the influence of the rf field on the discontinuity in dV/dI.

For sample 5, by synchronization experiments the satellites ν_1 and ν_2 appear from each side of the fundamental frequency ν_0 (Figs. 4 and 5). In Fig. 17 we have drawn the variation of ν_0/ν_1 and ν_0/ν_2 as a function of E/E_c. For the upper CDW, $\nu_0/\nu_1=1.50\pm0.03$ and $\nu_0/\nu_2=0.67\pm0.02$ up to $E/E_c\sim2.8$; then ν_0/ν_1 decreases slowly down to 1. For the lower CDW for $E/E_c\lesssim2$ we find that $\nu_0/\nu_1=1.50\pm0.03$ and $\nu_0/\nu_2=0.65\pm0.03$, and at high electric field the three frequencies converge together. Therefore it seems that for relatively small E/E_c ν_0,ν_1,ν_2 are in a constant ratio $\frac{3}{2}$ and $\frac{2}{3}$, and that above a certain value of E/E_c (which is not the same for the two CDW's) the three frequencies become increasingly closer to one another. This constant ratio between ν_0 and ν_1,ν_2 seems also to be induced by the rf field in the synchronization because by direct noise analysis the three frequencies are much more separated from one another near E_c.

IV. PHENOMENOLOGICAL MODEL

We want to discuss the properties of the motion of CDW's in our model when a domain or an array of domains defined by a probability distribution of

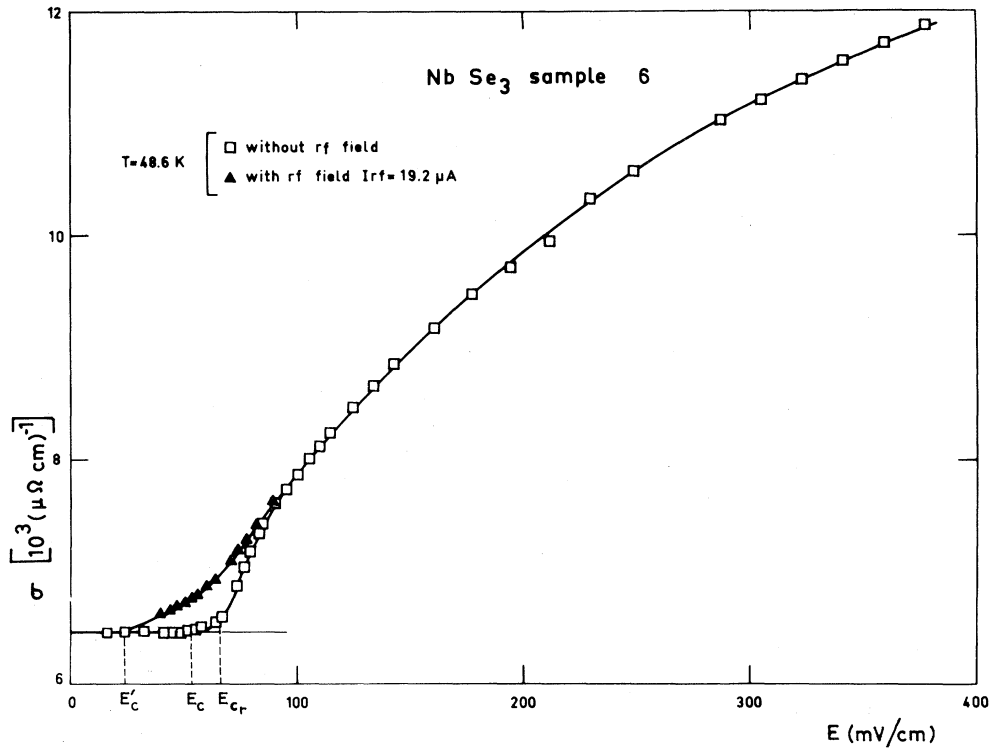

FIG. 14. Variation of the conductivity as a function of the electric field for sample B6 at $T=48.6$ K with and without rf field superposed.

critical fields is subjected to a continuous field E higher than the depinning field plus a weak time-dependent field $E_0(t)$. Special attention will be paid to the case where the perturbing weak field is periodic. We shall see that many experimental features can be interpreted, at least qualitatively, by this calculation.

A. Perturbation of the motion of a single domain

1. Perturbation of the motion of the wave by a weak time-dependent field

We recall here the equations obtained in Sec. IV B of paper I. [We keep the same numbers for the equations as in paper I, and we continue the numeration here in paper II. The new equations in paper II start at (25).] We have

$$\tau\frac{\partial\phi}{\partial t}=\frac{E}{E_c}+\sin\phi\ , \tag{9a}$$

$$j=\sigma\left[E+\beta E_c\tau\frac{\partial\phi}{\partial t}\right]\ . \tag{9b}$$

Let us call e and $e_0(t)$ the dimensionless variables E_{dc}/E_c and $E_0(t)/E_c$, $e_0<<1$.

We must solve

$$\tau\frac{\partial\phi}{\partial t}=e+\sin\phi+e_0(t)\ . \tag{25}$$

If we call ϕ_0 the unperturbed solution

$$\tau\frac{\partial\phi_0}{\partial t}=e+\sin\phi_0\ , \tag{26}$$

we can try for the solution

$$\phi=\phi_0+\epsilon\ . \tag{27}$$

Since e_0 is small, we can expect that ϵ is also, and develop to first order

$$\sin(\phi_0+\epsilon)=\sin\phi_0+\epsilon\cos\phi_0\ .$$

Substituting in (25) and using (26), one has

$$\tau\frac{\partial\epsilon}{\partial t}-\epsilon\cos\phi_0=e_0(t)\ . \tag{28}$$

This linearized equation can be solved by standard methods, ϕ_0 being a known function of t. The result is

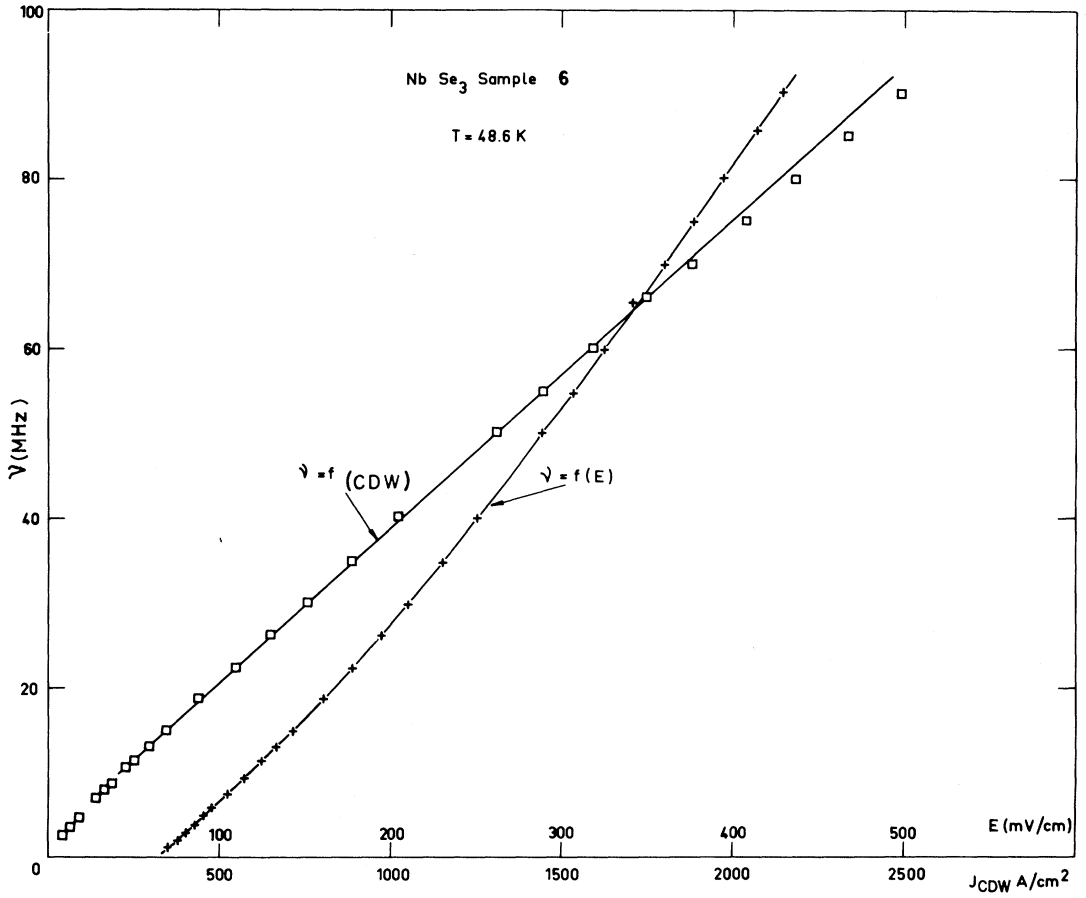

FIG. 15. Variation of the fundamental frequency ν_0 as a function of the electric field for large values of E. We have shown also the variation of ν as a function of the current carried by the J_{CDW}.

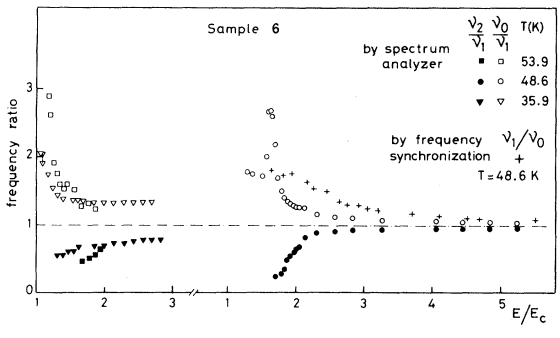

FIG. 16. Variation with E/E_c of the ratio between the satellite fundamental frequencies obtained in noise analyzer compared to the fundamental ν_0, the left-hand part: $T=35.9$ and 53.9 K. The right-hand part: $T=48.6$ K. The peak in ν_0/ν_1 at this temperature near E_c is a consequence of the discontinuous variation of dV/dI at this electric field.

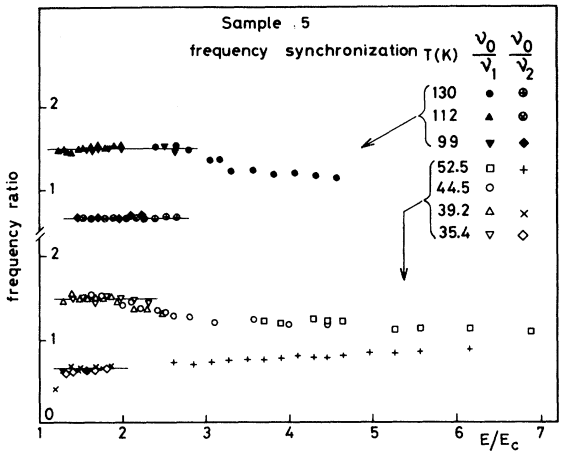

FIG. 17. Variation with E/E_c of the ratio between the satellite fundamental frequencies ν_1 and ν_2 compared with the fundamental ν_0 obtained by the synchronization experiment in sample 5. Upper part: upper CDW. Lower part: lower CDW. For $E_c < E \lesssim 2E_c$, ν_1 and ν_2 are practically $\frac{2}{3}\nu_0$ and $\frac{3}{2}\nu_0$.

$$\phi=\phi_0+\frac{1}{\tau}(e+\sin\phi_0)\int^t \frac{e_0(t)dt}{(e+\sin\phi_0)} . \quad (29)$$

The calculation can be considered as correct, unless the perturbing term $\phi-\phi_0$ becomes of the order of unity. Using formulas (14) and (15) of paper I, we see that $|e+\sin\phi_0|<e+1$ and that

$$|\epsilon|<\frac{e+1}{\tau}\int^t \frac{e_0(t)dt[e+\sin(\omega t+\psi)]}{e^2-1} .$$

Since $e_0(t)$ has no continuous component, and if $e>>1$, the only problem that can arise is associated with the integral of the product $e_0(t)\times\sin(\omega t+\psi)$ when $e_0(t)$ has a Fourier component at the natural frequency of the CDW.

2. *The important case of a periodic perturbation*

If

$$e_0(t)=e_0\cos\omega_0 t ,$$

even if $\omega_0\neq(e^2-1)^{1/2}/\tau=\omega$, where ω is the fundamental frequency of the modulated current [Eq. (11) in paper I], the integral contains a term in $1/(\omega-\omega_0)$ which magnifies the amplitude e_0. In this case we shall look for a forced oscillator behavior. Let us call a the reduced continuous field, which, if applied alone, would give exactly ω_0 for the natural motion frequency. Since $\omega\neq\omega_0$, $a\neq e$. Call ϕ_1 the solution of

$$\tau\frac{\partial\phi_1}{\partial t}=a+\sin\phi_1 \quad (30)$$

and try

$$\phi=\phi_1+\epsilon .$$

If ϵ is small, the same calculation as in Sec. IV A 1 gives

$$\tau\frac{\partial\epsilon}{\partial t}-\epsilon\cos\phi_1=e-a+e_0\cos\omega_0 t \quad (31a)$$

and

$$\phi=\phi_1+\frac{1}{\tau}(a+\sin\phi_1)\times\int^t \frac{e_0\cos\omega_0 t+(e-a)}{a+\sin\phi_1}dt , \quad (31b)$$

and from Eq. (14) in paper I,

$$\frac{1}{a+\sin\phi_1}=\frac{1}{a^2-1}[a+\sin(\omega_0 t+\psi)] .$$

Thus the continuous part of the function to be integrated contains $a(e-a)$ and the mean value of

$$\langle e_0\cos\omega_0 t\sin(\omega_0 t+\psi)\rangle_{av}=\frac{e_0}{2}\sin\psi .$$

This continuous part must vanish, and therefore we have the phase relations

$$\sin\psi=\frac{2a(e-a)}{e_0} , \quad (32a)$$

$$\cos\alpha=-\frac{2a(e-a)}{e_0} , \quad (32b)$$

where we have made use of Eq. (16) of paper I, which gives the phase of the fundamental frequency of the current $\tau d\phi/dt$ equal to $\alpha=\psi+\pi/2$, α being the relative phase between the current at ω_0 carried by the solution ϕ_1, and the exciting field at the same frequency. Solutions can only be found between e_m and e_M, the phase factor varying from $+1$ to -1, and $\alpha=\pi/2$ if $e=a$ (Fig. 18). This variation is to be expected from energy considerations: If, for example, $e<a$, the natural frequency will be lower than the applied ω_0, but the motion with the forced oscillator is at ω_0. The mean velo-

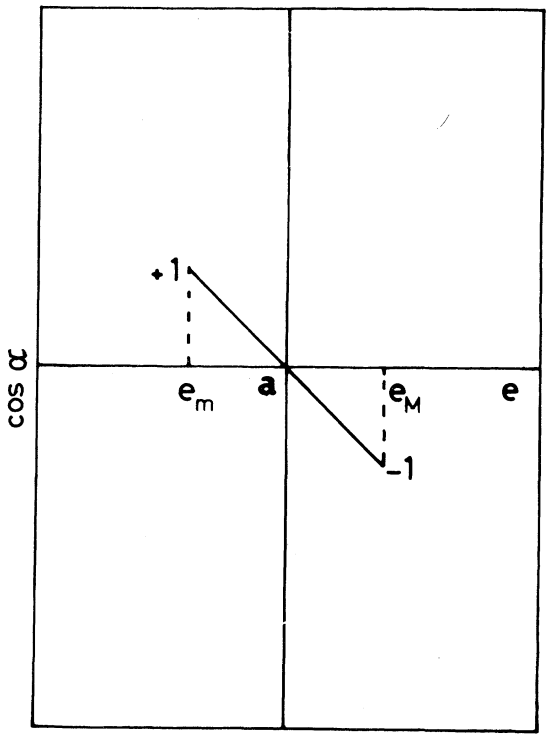

FIG. 18. Variation of the relative phase α between the rf exciting field $e_0\cos\omega_0 t$ and the current at the same frequency with $\cos\alpha$ defined in Eq. (32b).

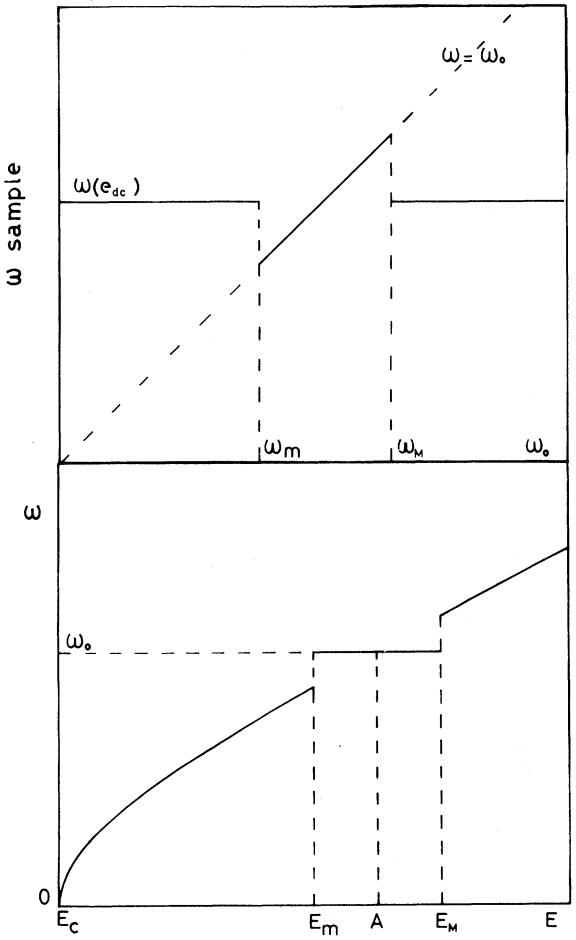

FIG. 19. (a) Variation of ω with the electric field. If A is the electric field corresponding to the applied rf frequency ω_0, synchronization takes place in the range between e_m and E_M. (b) In the frequency range between ω_m and ω_M the eigenfrequency in the domain is locked on the rf external ω_0 frequency.

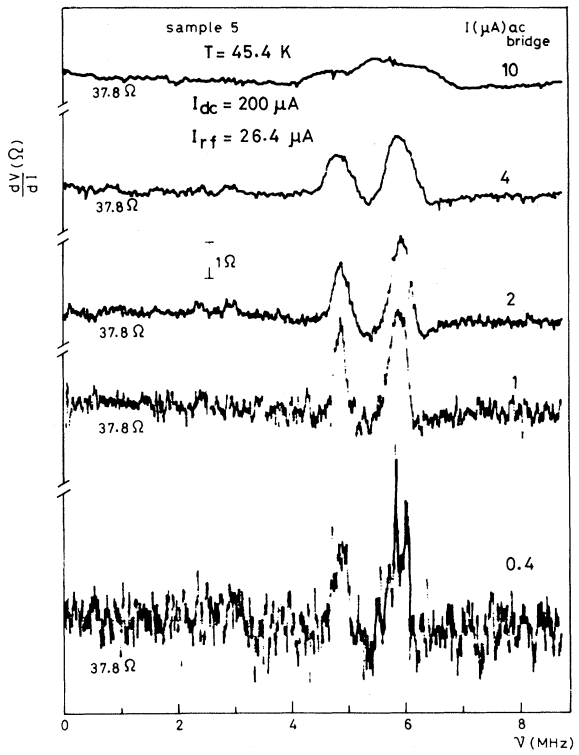

FIG. 20. Variation of the differential resistance dV/dI as a function of the external rf field for a constant electric field at different current of the 33-Hz ac bridge. Peaks disappear for $I_{33\ \mathrm{Hz}} \sim 10\ \mu$A, which corresponds to the suppression of the synchronization frequency range shown in Fig. 19(b).

city is higher and the rf field has to push the wave to overcome damping. This corresponds to an electrical power

$$|j_\sim| \, |e_0| \cos\alpha > 0 \, .$$

Of course, if one increases e_0, linearization is no longer justified; but ϵ has a strong periodic component at ω_0, and

$$\sin(\phi_1+\epsilon_0) \neq \sin(\phi_1 + |\epsilon_0| \sin\omega_0 t) = \sum_k J_k |\epsilon_0| \sin(\phi_1 + k\omega_0 t) \, .$$

Synchronization can occur if ϕ_1 has a component at $n\omega_0$ (n being an integer), so that for the fundamental frequency mixing, ω_0 appears as a subharmonic of the fundamental frequency of ϕ_1.

3. *Explanation of the peaks in dV/dI when a dc field E and a rf field ($E = E_0 \cos\omega_0 t$) are superposed — case of a single domain*

On the curve $\omega(E)$ of Fig. 19(a), we plot the field A corresponding to the applied rf frequency ω_0. For a given rf amplitude, synchronization occurs in the range between E_m and E_M. But since ω is proportional to the velocity, it is also proportional to the dc current carried by the CDW. If we apply small variations of E between E_m and E_M, since $\omega = \omega_0$, the δj_{CDW} does not change. δI associated with δV is only due to the Ohmic conduction, giving a peak in the dV/dI curve equal to the Ohmic value. The center of the peak is independent of the rf amplitude, and the width increases with the rf amplitude. If one increases the rf amplitude, subharmonic and harmonic peaks can appear. By increasing the amplitude, the first peak to appear

corresponds necessarily to the fundamental frequency. This is important in order to label correctly the fundamental frequency in complicated spectras.

In order to increase the sensitivity, most of the experiments have been performed at constant dc field and by slowly sweeping the frequency. For a given amplitude that is not too large we shall have a frequency range between ω_m and ω_M in which the eigenvalue in the domain is locked on the rf external frequency [Fig. 19(b)]. If we change slightly the electric field E delivered at 33 Hz by the ac bridge for the dV/dI measurement, frequency remains monitored by the rf field, and there is no CDW current given for this small excess dV. Thus in the lock-in detection we have no 33-Hz component for the CDW current, and we may recover the Ohmic value.

In Fig. 20 we show the variation of dV/dI as a function of the external frequency for a constant dc field and with different currents delivered at 33 Hz by the ac bridge. It is to be noted that for sufficiently high 33-Hz current, say a rms value of 7 μA or an amplitude of 10 μA, the peaks have totally disappeared.

This is easy to understand with the help of Fig. 19(b): If the variation of E due to the dV/dI measurement exceeds the locking value corresponding to ω_m or ω_M, we shall recover motion of the CDW no longer modulated by the rf field, but by the applied field on a noticeable fraction of the cycle. The result will be a dynamical impedance between the Ohmic value and its value in the absence of rf field. Since the dynamical resistance is 40 Ω, the ac field at 33 Hz has an amplitude of 0.40 mV. Formula (32b) gives for the extreme e value

$$e-a=\frac{e_0}{2a}\rightarrow E-E_A=E_c\left[\frac{E_0}{2E_A}\right].$$

The limit is obtained for $E-E_A=E_{33\text{ Hz}}=0.40$ mV. E_0 is the amplitude of the rf field. 2.35 mV, and in this case $E_c=4.32$ mV, $E_A/E_c=2.74$, so that

$$E_c\left[\frac{E_0}{2E_A}\right]=2.35\frac{1}{2(2.74)}=0.43\text{ mV}$$

to be compared to 0.40 mV, amplitude of the 33-Hz bridge. It should be noted that this exceptionally good agreement is quite model independent: Every nonlinear equation will give a frequency locking, and the factor 2 in the equation is associated with $\langle\sin^2\omega t\rangle=\frac{1}{2}$.

B. Many-domain self-synchronization and periodic components of the noise at regulated dc field

To interpret, at least qualitatively, the shape of the dc dV/dI curve, in paper I we have had to introduce a Gaussian distribution of critical fields inside a given sample. If we neglect every correlation from domain to domain, the result will be a sum of currents, each one reflecting its own frequency in the given dc field, with arbitrary phases which are equivalent to a noise with a spectrum centered at the frequency associated with the mean value E_M of the probability distribution, and a width reflecting its standard deviation s.

To explain discrete frequencies, especially low discrete frequencies, we have to introduce interaction between domains and look for a self-synchronization of many domains on their own rf field, even in the absence of applied external ac current.

In the presence of a dc field E and of depinned domains, the magnetic equivalent model developed in Sec. IV C of paper I still holds, and a mean-field approximation will lead to the use of mean values of the Ohmic current density, electric field, and CDW current density. This was achieved in Sec. IV C of paper I for the dc components. But since j_{CDW} has not only continuous but also a fundamental and harmonic frequency term, we can introduce an ac component for the "magnetization" with corresponding ac components for the electric field: $E_0\cos\omega_0 t$, the Ohmic current, and so on. If we assume that the domains are elongated enough,

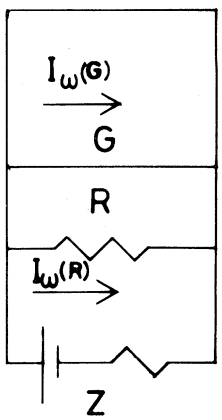

FIG. 21. Schematic diagram of a depinned domain: a nonlinear generator connected to the Ohmic resistance of the sample and the dc generator with a very high internal impedance.

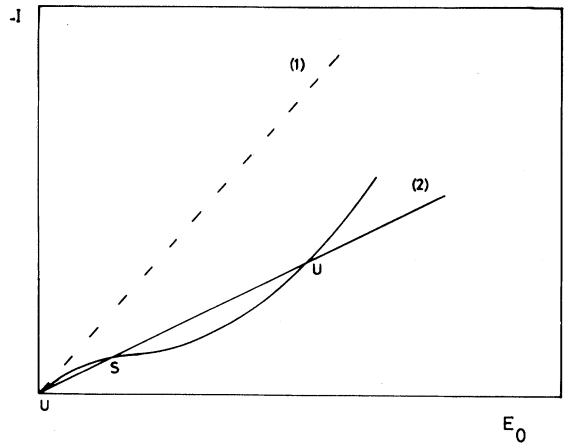

FIG. 22. Schematic solutions of Eq. (34). In case (1) there is no self-synchronization. In case (2), the self-synchronization takes place in S, and well-defined frequencies will be observable in the crystal.

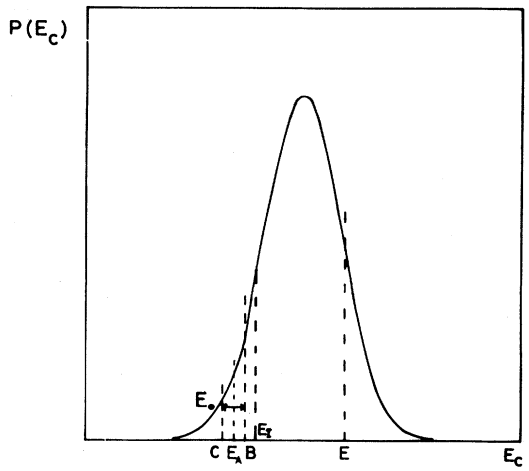

FIG. 23. Gaussian distribution of the critical electric fields of the assembly of domains. E is the applied electric field, E_A the critical field which gives the frequency ω_0 in the applied field E. Self-synchronization will take place between B and C.

"demagnetizing coefficients" disappear, and for dc and ac components,

(i) the field on each domain is equal to the mean field, and

(ii) the mean CDW current is the integral of the normalized probability, multiplied by the current delivered by each depinned domain.

We have seen that for weak E_0, synchronization can only occur when the fundamental frequency is near ω_0. Therefore, harmonic terms in the CDW current give rise only to harmonic terms in the electrical field, without further perturbation on the motion. They can be neglected in the following discussion.

At a given ω_0, if there is synchronization, the depinned domains are equivalent, as shown in Fig. 21, to a nonlinear generator G, connected to the Ohmic resistance R of the sample and to the dc generator through a very high impedance Z. By current conservation one has

$$i_\omega(G)+i_\omega(R,Z)=0 \tag{33}$$

i_Z can be neglected, and since R is purely resistive, with the remarks we have made above, one can transform this equation as

$$\int \left| j_{\mathrm{CDW}}^{\mathrm{ac}} \right| \cos\alpha p(E_c)\,dE_c+\sigma E_0=0\ , \tag{34}$$

where α is the phase angle between E_0 and j_{CDW} at ω_0, and where $|j_{\mathrm{CDW}}|$ and $\cos\alpha$ are functions of E_0. Calling the integral I, the plot of σE_0 and of $-I$ as schematized in Fig. 22 gives the following solutions [in case (1) there is no self-synchronization; in case (2) self-synchronization takes place in S]:

$E_0=I=0$ in case (1);

Three intersection points in case (2).

Since the driving term is $-I$ and the resistive term σE_0, discussion of the stability of the equilibrium shows that only point S is stable: In this case we get self-synchronization.

1. *Domain of synchronization for a given E_0*

Since we need the integral I for a given E_0, we have to see what is the domain of synchronization in a given E. The problem is slightly different from that of Sec. IV A 2, where for a given domain one varies the dc field E. Here E is given, and the critical field of the domains varies following the probability law: We look at the range of critical fields which are self-synchronized by $E_0\cos\omega_0 t$.

If we remember that in paper I, we have shown that for a given domain j

$$E_{c_j}=\frac{f_j}{n'e}\ , \tag{6}$$

$$\tau_j=\frac{\eta}{f_j}\ . \tag{7}$$

Since η and $n'e$ are the same for all domains, f_j being different from domain to domain, one can define τ_M as the time constant associated with the mean value of the critical fields E_M, and write

$$\tau_j=\tau_M\frac{E_M}{E_{c_j}} . \tag{35}$$

The equation of motion of the phase becomes

$$\tau_M E_M\frac{\partial\phi}{\partial t}=E_c\sin\phi+E+E_0\cos\omega_0 t . \tag{36}$$

We can define the critical field E_A, such that it gives in the applied field E exactly the frequency ω_0:

$$\tau_M E_M\frac{\partial\phi_1}{\partial t}=E_A\sin\phi_1+E$$

and look for the solution

$$\phi=\phi_1+\epsilon .$$

The calculation is quite analogous to that of Sec. IV A 2. The result is that the phase between $\partial\phi_1/\partial t$ and E_0 must be equal to

$$\cos\alpha=2\left[\frac{E_A-E_c}{E_0}\right] \tag{37}$$

Therefore we have the following features (Fig. 23):

(1) Every domain in the range of critical fields,

$$E_A-\frac{E_0}{2}<E_c<E_A+\frac{E_0}{2} ,$$

is self-synchronized.

(2) The synchronization frequency corresponds to the natural frequency of the dc field E, for a critical field at the middle of this range.

(3) The modulus of the ac component of j_{CDW} is essentially that of the solution without ac field for the critical field E_A.

(4) There is also a weak contribution of $\partial\epsilon/\partial t$, the perturbation of the solution ϕ_1, which is proportional to E_0, the exciting ac field.

2. *Contribution of nonsynchronized domains to the ac synchronized current*

For critical fields higher than C or lower than B, the domains are not synchronized and work on their own frequency. However, the perturbation due to the mean ac field exists. Formula (29) applies in this case:

$$\frac{\partial\epsilon}{\partial t}=\frac{1}{\tau_0}e_0\cos\omega_0 t + \frac{1}{\tau}\frac{d}{dt}(e+\sin\phi_0)\int^t\frac{e_0\cos\omega_0 dt}{e+\sin\phi_0} .$$

The first term is a resistive one. However, since

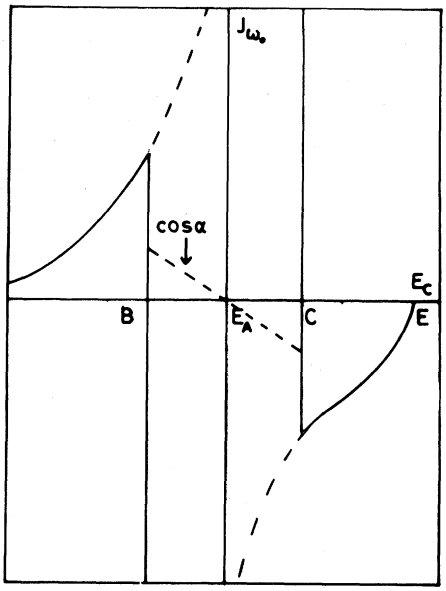

FIG. 24. Schematic contribution to the ac synchronized current j_{ω_0} for the domains where the critical electric fields is higher than C or lower than B. Between B and C every domain is self-synchronized.

$$(e+\sin\phi_0)^{\pm1}$$

have components at the true frequency of the given domain, by mixing, the integral will contain $|\omega_0\pm\omega|$, and the product, a component at $\omega_0=\omega_0\pm\omega\mp\omega$.

A straightforward calculation gives

$$j_{\omega_0}=\beta\sigma E_0\cos\omega_0 t\frac{K}{2(e^2-1)^{1/2}}\frac{\omega^2}{\omega^2-\omega_0^2} = |j_\omega|\frac{E_0\cos\omega_0 t}{4E_c}\left[\frac{1}{e^2-e_1^2}\right] , \tag{38}$$

where ω is the frequency of the domain, $|j_\omega|$ the modulus of the unperturbed solution for the domain, $e=E/E_c$, $e_1=E/E_A$, and K was defined in Eq. (17) in paper I.

At C one has

$$E_B=E_A+\frac{E_0}{2} ,$$

so that, for weak E_0:

$$j_{\omega_0}|_C\simeq-\frac{|j_\omega(C)|}{4}\left[\frac{E_A}{E}\right]^2 .$$

Since $E_A/E<1$, the perturbation is small, compared to the unperturbed current: Perturbation calculation still holds. The schematic variation of Eq. (38) is drawn in Fig. 24.

3. *Frequency locking for high applied fields E*

If a frequency locking appears, Eq. (34) has to be verified. The integral $-I$ will contain three contributions:

(a) A contribution of the phase-locked domains between B and C: $\partial\phi_1/\partial t$.

(b) A contribution of the perturbing $\partial\epsilon/\partial t$ in the same range.

(c) A contribution due to the $\partial\epsilon/\partial t$ value for the domains in the wings, outside the range BC.

(a) and (b) give, for small E_0, contributions to $-I$ proportional to E_0^2 and are unable to explain locking. For (a),

$$I_{(a)}=\int_{E_A-E_0/2}^{E_A+E_0/2}p(E_c)dE_c 2\left[\frac{E_A-E_c}{E_0}\right]|j_{\omega_0}(E_A)|\ ,$$

but

$$p(E_c)=p(E_A)+(E_c-E_A)p'(E_A)\ .$$

By parity $p(E_A)$ gives 0, and

$$I_{(a)}\simeq\frac{2}{3}|j_{\omega_0}(E_A)|p'(E_A)\left[\frac{E_0}{2}\right]^2\ .$$

For contribution (b), as noticed, ϵ between B and C is proportional to E_0, and since the width of integration is E_0, the integral, whatever the phase of ϵ, is at most like E_0^2.

However, for contribution (c), we have a net current at B or C, independent of E_0 due to the amplification term $\omega^2/(\omega^2-\omega_0^2)$. If E is a few times the critical field, $|j_\omega|$ becomes j_0, independent of E_c as seen in Sec. IV B 3 of paper I and shown in Fig. 9 of paper I. Hence the contribution is

$$I_{(c)}=\frac{j_0}{4}\frac{E_0\cos\omega_0 t}{E_A}\left[\int_{-\infty}^{E_A-E_0/2}f\,dE_c+\int_{E_A+E_0/2}^{\infty}f\,dE_c\right]\ , \quad (39)$$

with

$$f=p(E_c)\frac{E_c^2E_A^2}{E^2(E_A^2-E_c^2)}\ .$$

By changing the variable

$$E'=E_c-E_A$$

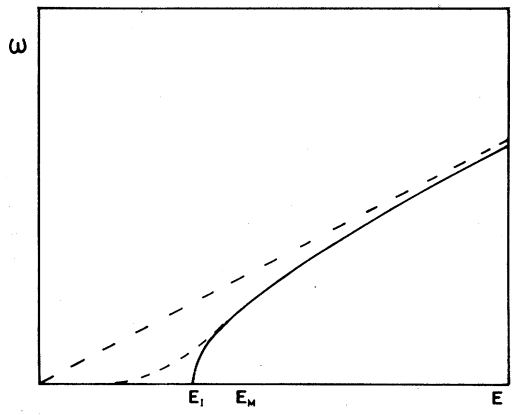

FIG. 25. Schematic variation of $\omega(E)$ with the self-synchronization of the domains in the sample. Our model might give an inflection point near E_M, but experimentally we observe an upward curvature.

we have

$$I_{(c)}=-\frac{j_0}{4}\frac{E_0\cos\omega_0 t}{E_A}\left[\frac{E_A}{E}\right]^2\times\int_{E_0}^{\infty}\frac{dE'}{E'}\left[p(E_A+E')\frac{(E_A-E')^2}{2E_A-E'}-p(E_A-E')\frac{(E_A+E')^2}{2E_A+E'}\right]\ .$$

However, the probability $p(E_A\pm E')$ is important only in the range of s which is $<<E_A$. Therefore $(E_A\pm E')/(2E_A\pm E')\cong E_A/2$ in the domain where p has some weight. In the limit $E_0\to 0$ the integral has a nonzero and convergent value and

$$I_{(c)}\cong-\frac{j_0}{4}E_0\cos\omega_0 t\left[\frac{E_A}{E}\right]^2\times\int_0^{\infty}\frac{dE'}{E'}[p(E_A+E')-p(E_A-E')]\ . \quad (40)$$

We have now a linear term in E_0 which can overshoot the resistive term σE_0 of Fig. 22. If this is the case, we are dealing with case (2), and one can expect a self-synchronization, the origin $(E_0=I=0)$ becoming unstable.

Since the important part of the integral in (40) is for small values of E_c, *its maximum is obtained for* E_A *very near the rising inflection point* E_I of the repartition curve. This point then corresponds to the higher ac level, and is probably the most stable. The integral is of the order of $1/s$, and moreover,

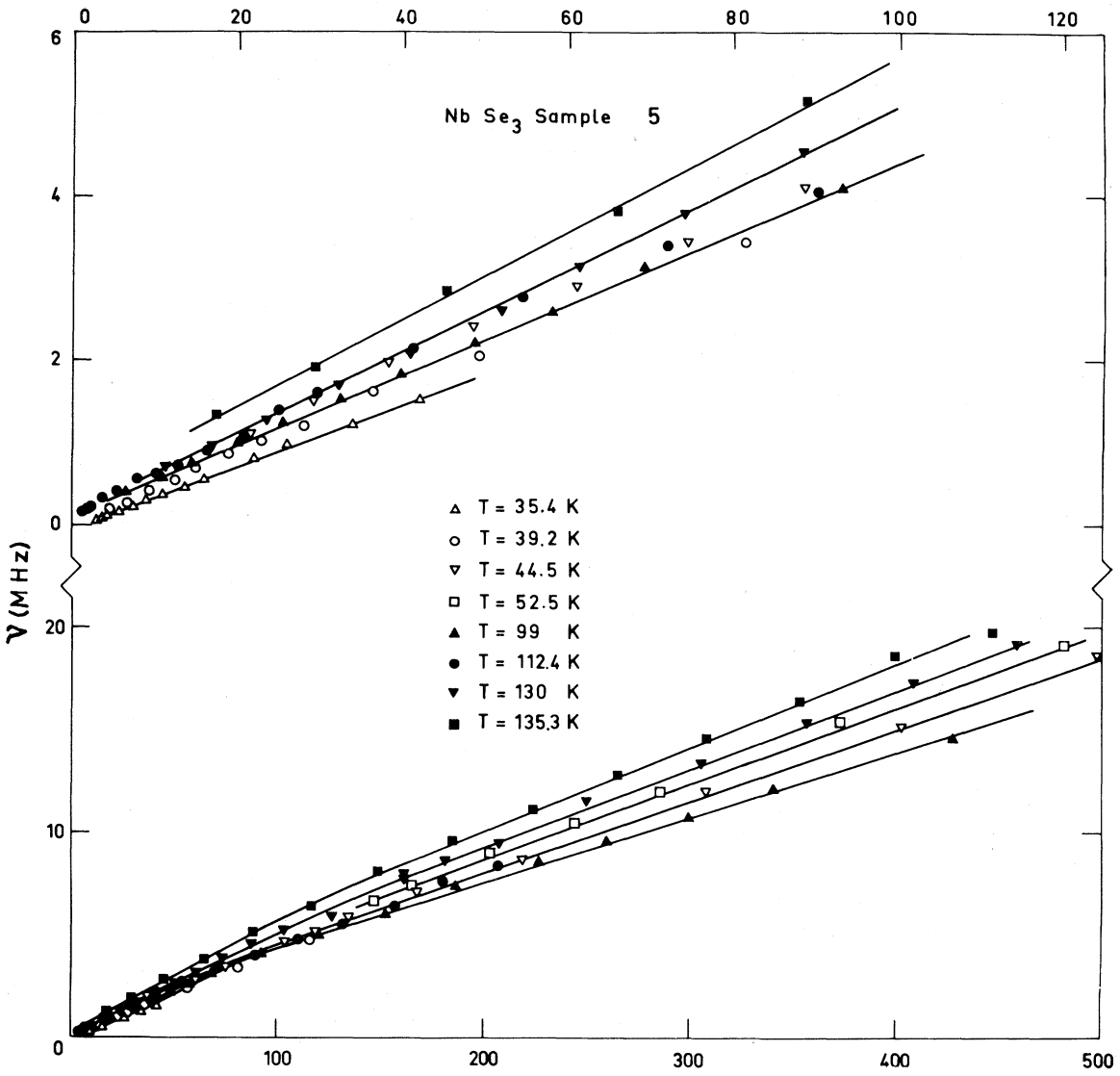

FIG. 26. Variation of the fundamental frequency ν_0 in the noise for sample 5 as a function of J_{CDW}, the current density carried by the CDW for the two CDW's. Upper part: $J_{CDW} < 100$ A/cm^2. Lower part: J_{CDW} up to 400 A/cm^2. The $\nu(E)$ curves for the same temperatures were drawn in Fig. 11. The inverse of the slope of $\nu(J_{CDW})$ is proportional to the number of electrons condensed by the CDW gap.

$$j_0 = \beta\sigma E_A \ .$$

Self-synchronization will appear only if

$$\tfrac{1}{4}\beta \frac{E_A}{s}\left[\frac{E_A}{E}\right]^2 \gtrsim 1 \ .$$

Even if $E_A/s \sim 20$, $\beta \sim 2$, $E < 3E_A \sim 3E_c$, three times the critical field. However, self-synchronization has been observed for higher fields, say $10E_c$.

By decreasing the applied dc field E, $|j_\omega|$ becomes a function of E_c, and the integral is much more complicated, so that E_A becomes a complicated function of E_{dc}. However, one cannot expect variations of E_A higher than a few standard deviations s of the statistical law, below the inflection point, so that the best fit one can hope for with the experimental $\omega(E)$ is a pronounced inflection point near E_M (as drawn in Fig. 25). However, experimentally $\omega(E)$ shows an upward curvature.

Since harmonics have been seen in very high fields, one possible explanation could be that the law of motion in true domains is different from

TABLE II. Electronic concentration condensed by the CDW formation. These numbers are obtained from the slope of $\nu(J_{CDW})$ in two different J_{CDW} ranges for several temperatures and different samples. The results for sample 1 were previously shown in Ref. 12 (sample labeled B2).

Sample	T (K)	n (10^{21} cm^{-3}) $J<100$ A/cm^2	n (10^{21} cm^{-3}) $J>100$ A/cm^2
5	35.4	1.23	
	39.2	1.11	
	44.5	0.91	1.33
	52.5	1.10	1.25
	99	1.08	1.46
	112.4	0.94	
	130.0		1.23
	135.3	0.86	1.13
6	35.9	0.77	
	48.6	0.78	1.28
	53.9	0.64	
1	47.0	0.83	
2	47.0	1.30 (ν_0)	
		0.86 (ν_1)	
3	46.0	1.33 (ν_0)	
7	45.5	0.86 (ν_0)	

that we have chosen with higher contributions both for the fundamental frequency and for the harmonics, compared to the continuous contribution.

V. DISCUSSION

The two basic equations of our model were derived in paper I. We have calculated the current J_{CDW} carried by the CDW as a function of the electric field, and we have shown that this current is the superposition of a continuous current and a modulation where the fundamental frequency as a function of E is given by Eq. (11). However, J_{CDW} can be directly related to the frequency ν by the model-independent relation

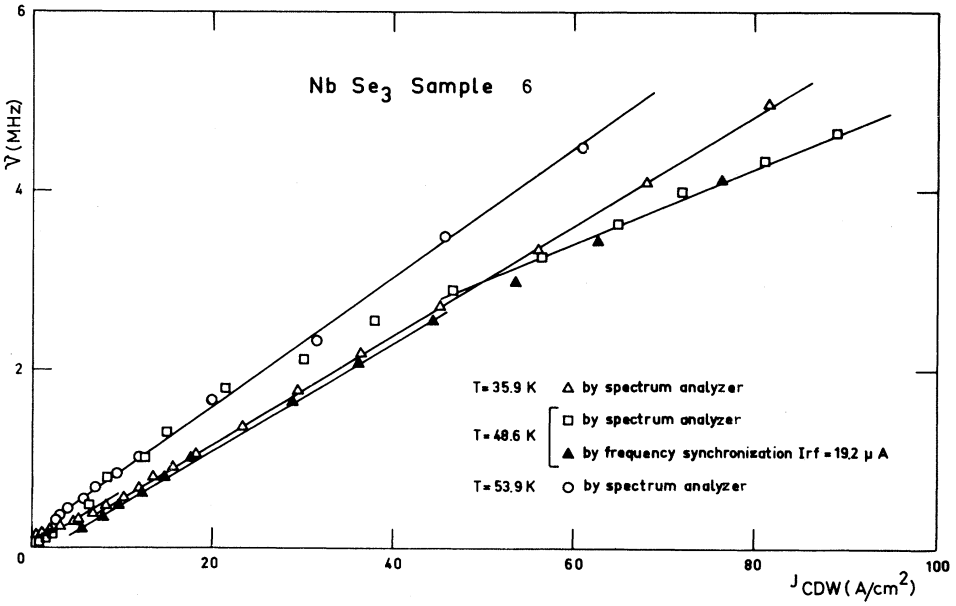

FIG. 27. Variation of the fundamental frequency ν_0 in the noise as a function of J_{CDW} for sample 6 for the lower CDW.

$$J_{CDW} = -n'ev \ ,$$

where $n'e$ is the number of electrons affected in the band by the CDW gap and $v = 2\pi\nu/Q$, where Q is the CDW wavelength. Thus

$$\nu = \frac{Q}{2\pi}\frac{1}{n'e}J_{CDW} \ . \tag{41}$$

J_{CDW} can be obtained directly by measuring the nonlinear characteristics $V(I)$. We assume that

$$J_{CDW} = J\left[1 - \frac{R}{R_n}\right] , \tag{42}$$

where J is the applied current density, R the resistance for this J value, and R_n the Ohmic resistance for $J \sim 0$. In the direct noise analysis we have measured for each temperature the resistance R as a function of E.

To account for the effect of the rf field in the synchronization experiment, as seen in Fig. 14, we have measured R with a rf field of 100 kHz with the same amplitude as that used in the dV/dI experiments. The cross section of the samples taken for the calculation of J_{CDW} is deduced from the room-temperature resistance assuming the same resistivity of 250 $\mu\Omega$ cm for all the samples. In Fig. 26 we have drawn ν as a function of J_{CDW} for sample 5 at seven temperatures involving the two CDW's, the upper part of Fig. 26 for low J_{CDW} current densities, and the lower part for large extensions of J_{CDW}. The $\nu(E)$ curves for the same temperatures were shown in Fig. 11. We note that all the $\nu(E)$ curves for the two CDW's, when plotted as a function of J_{CDW}, gather in a compact pattern. ν is linear with J_{CDW} up to around 100 A/cm^2 and shows a slight curvature for higher J_{CDW}. We want also to point out that for each CDW the slope of $\nu(J_{CDW})$ is higher when T reaches T_{c_1} or T_{c_2}. The inverse of this slope is proportional to n', the number of electrons in the band affected by the CDW gap. The values of n' deduced from our measurements are in Table I in the low J_{CDW} limit and in the high J_{CDW} limit ($J > 100$ A/cm^2). Near T_{c_1} and T_{c_2} the CDW gap is not totally established and n' has a smaller value than at lower temperature.

In Fig. 27 we show the same $\nu(J_{CDW})$ for sample 6. The break in $\nu(E)$ at $T = 48.6$ K as seen in Fig. 13 due to the rounding in dV/dI before its fast decrease is suppressed when ν is plotted as a function of J_{CDW}, and we obtain again a linear variation. The slopes for sample 6 are a little higher than those for sample 5. Finally, in Fig. 28 we have plotted ν_0, ν_1, and ν_2 as a function of J_{CDW} for five samples at the temperature where the resistivity is maximum for the lower CDW. There is some dispersion which can be considered as reasonable if we take into account the error in the measurements of the dimensions of the samples. It can be noted also that the sample doped with tantalum impurities follows the same variation as the pure one.

Following the discussion in paper I, we consider that at room temperature only four chains participate in the conduction with 0.5 electron at room temperature per niobium. We have deduced that the total numbers of electrons is therefore $n = 3.9 \times 10^{21}$ cm^{-3}. As two chains are involved in each CDW, before the distortion at room temperature $n = 1.95 \times 10^{21}$ cm^{-3}. We find that for each CDW the number of electrons affected by the gap is around 1.0×10^{21} cm^{-3}. If we had taken $\rho = 150$ $\mu\Omega$ cm as measured by Ong and Gould[15] for each CDW, n' would be $\sim 1.7 \times 10^{21}$ cm^{-3}.

The low-temperature specific heat of $NbSe_3$ has been recently measured.[16] Between 0.15 and 1 K the electronic contribution to the specific heat is $\gamma = 24.5$ erg/g K^2. If we assume a free-electron mass for the carriers at low temperature, we can deduce that the number of electrons below the two CDW's is around 0.98×10^{21} cm^{-3}. Therefore we get a consistent picture for $NbSe_3$: The room-temperature electron concentration is assumed to be 3.9×10^{21} cm^{-3} (from band calculations). An equal number of electrons around $(1-1.2) \times 10^{21}$ cm^{-3} is condensed below each CDW gap (from our measurements described above) and 25% of conduction electrons remains approximately at low temperature (from specific-heat measurements).

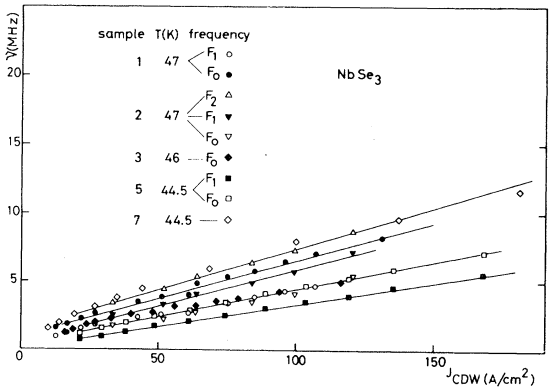

FIG. 28. Variation of the fundamental frequencies ν_0 and ν_1, ν_2 in the noise as a function of J_{CDW} for the lower CDW at the temperature where the resistivity is maximum for five different samples.

VI. CONCLUSIONS

In these two papers, we have measured for many samples the differential resistance dV/dI as a function of the electric field, studied the noise generated above E_c, and performed synchronization of this noise by an external rf field. We have noted that the two CDW's which take place in $NbSe_3$ behave similarly. It appears well established that the non-Ohmicity of $NbSe_3$ is due to the motion of the CDW's. We have explained that the pinning force which modulates the current has a periodicity 2π in $\phi(r_i)$ where r_i is the position of the impurity. A sufficient electric field is necessary to overcome the pinning energy. Above this critical field the current is formed by the superposition of a continuous current and a modulation with a fundamental frequency and harmonics. We have shown that the frequency is a linear function of the current carried by the CDW and deduced the number of electrons affected by the CDW gap in excellent agreement with band calculations.

We have developed a model where the phase of the CDW is described by an overdamped oscillator. This model explains qualitatively the shape of the dV/dI curves as shown in paper I and the synchronization of the noise by an external rf field and the observation of peaks induced in the dc dV/dI characteristics by the rf field (Sec. III A in paper II). We have also described the principle of the self-synchronization of all the domains to give well-defined frequencies in the noise spectrum.

However, with this model we encounter some problems when we want to obtain a quantitative agreement with the experimental results. We have seen in paper I that the shape of dV/dI varies very rapidly with T for the lower CDW. To explain this behavior we have to make the hypothesis of a change of the size of the domains at low temperature, in a temperature range where the coherence length of the CDW does not vary anymore. Our model gives a downward curvature in the variation of v with the electric field. We show in Sec. IV B 3 of paper II that, in the synchronization of the domains, we can obtain a strong inflection point for the electric field when the electric field distribution is maximum. However, our experimental results show an upward concavity in the whole range (Figs. 11 and 12). Finally, the calculations indicate that the harmonics in the noise must decrease rapidly (paper I, Fig. 9), but experimentally, harmonics are detectable at $10E_c$.

These difficulties lead us to criticize the model we have used. As noted by Sokoloff,[17] the kind of overdamped nonlinear equation that we have derived will always give an infinite dv/dE near the critical field for a single domain. The existence of domains with well-defined walls is not proven. Others' models are much more difficult to study, like a continuous $\phi(r,t)$ in the bulk or a $\phi(r,t)$ with dislocations or solitons, and therefore it is impossible to compare them with experiment. In fact, we have treated the CDW lattice as a polycrystal, but another method would be to treat the CDW lattice as a crystal with dislocations. Our model gives a unique fundamental frequency, but experimentally all the Fourier spectrum is described with three fundamental frequencies. Nonlinear solutions of a damped oscillator submitted to an external rf field has been studied recently[18] by varying the frequency ω and the amplitude Γ. The $\Gamma(\omega)$ diagram is rather complicated but shows zones of periodic solutions and bifurcation to chaotic regime. Such a behavior might be applicable to $NbSe_3$. Finally the treatment of the domains in a mean-field approximation especially for the transport properties like dV/dI is not very satisfying. Percolation would be more suitable and could perhaps explain the rapid drops of dV/dI when enough domains begin to move, especially for high β values, i.e., at low temperatures.

ACKNOWLEDGMENTS

We would like to thank L. Guemas, A. Meerschaut, and J. Rouxel from the Laboratoire de Chimie Minérale de Nantes for providing us with the samples, J. Bret for his help with the electronics, M. Papoular for helpful discussions, and J. Bardeen, R. M. Fleming, N. P. Ong, and J. W. Steeds for sending their papers before publication.

[1]J. Bardeen, L. N. Cooper, and J. R. Schrieffer, Phys. Rev. 108, 1175 (1957).

[2]H. Frölich, Proc. R. Soc. London Ser. A 223, 296 (1954).

[3]P. A. Lee, T. M. Rice, and P. W. Anderson, Solid State Commun. 14, 703 (1974).

[4]P. Brüesch, S. Strässler, and H. R. Zeller, Phys. Rev. B 12, 219 (1975).

[5]A. J. Heeger, in *Highly Conducting One-Dimensional Solids,* edited by J. T. Devreese (Plenum, New York,

1979), p. 69.
[6]A. Andrieux, H. J. Schulz, D. Jerome, and K. Bechgaard, Phys. Rev. Lett. 43, 227 (1979).
[7]P. Monceau, J. Richard, and M. Renard, preceding paper, Phys. Rev. B 25, 931 (1982), and references cited therein.
[8]J. Bardeen, in *Highly Conducting One-Dimensional Solids,* edited by J. T. Devreese (Plenum, New York, 1979), p. 373.
[9]R. Fleming and C. C. Grimes, Phys. Rev. Lett. 42, 1423 (1979).
[10]K. K. Fung and J. W. Steeds, Phys. Rev. Lett. 45, 1696 (1980).
[11]P. Haen, J. M. Mignot, P. Monceau, and M. Nunez-Regueiro, J. Phys. (Paris) Colloq. 39, C6-703 (1978).
[12]P. Monceau, J. Richard, and M. Renard, Phys. Rev. Lett. 45, 43 (1980).
[13]R. Fleming, Phys. Rev. B 22, 5606 (1980).
[14]M. Weger, G. Grüner, and W. G. Clark, Solid State Commun. 35, 343 (1980).
[15]N. P. Ong and C. M. Gould, Solid State Commun. 37, 25 (1981).
[16]J. C. Lasjaunias and P. Monceau (unpublished).
[17]J. B. Sokoloff, Phys. Rev. B 23, 1992 (1981).
[18]B. A. Huberman and J. P. Crutchfield, Phys. Rev. Lett. 43, 1743 (1979); B. A. Huberman, J. P. Crutchfield, and N. H. Packard, Appl. Phys. Lett. 37, 750 (1980).